Mineralogy and Petrology (2018) 112 (Suppl 2):S609–S624
https://doi.org/10.1007/s00710-018-0562-2

ORIGINAL PAPER

The P3 kimberlite and P4 lamproite, Wajrakarur kimberlite field, India: mineralogy, and major and minor element compositions of olivines as records of their phenocrystic vs xenocrystic origin

Azhar M. Shaikh[1] · Satya P. Kumar[1] · Suresh C. Patel[1] · Satyajeet S. Thakur[2] · Subramanian Ravi[3] · Duryadhan Behera[4]

Received: 15 November 2017 / Accepted: 27 February 2018 / Published online: 26 March 2018

Abstract

Distinctly different groundmass mineralogy characterise the hypabyssal facies, Mesoproterozoic diamondiferous P3 and P4 intrusions from the Wajrakarur Kimberlite Field, southern India. P3 is an archetypal kimberlite with macrocrysts of olivine and phlogopite set in a groundmass dominated by phlogopite and monticellite with subordinate amounts of serpentine, spinel, perovskite, apatite, calcite and rare baddeleyite. P4 contains mega- and macrocrysts of olivine set in a groundmass dominated by clinopyroxene and phlogopite with subordinate amounts of serpentine, spinel, perovskite, apatite, and occasional gittinsite, and is mineralogically interpreted as an olivine lamproite. Three distinct populations of olivine, phlogopite and clinopyroxene are recognized based on their microtextural and compositional characteristics. The first population includes glimmerite and phlogopite–clinopyroxene nodules, and Mg-rich olivine macrocrysts (Fo 90–93) which are interpreted to be derived from disaggregated mantle xenoliths. The second population comprises macrocrysts of phlogopite and Fe-rich olivine (Fo 81–89) from P3, megacrysts and macrocrysts of Fe-rich olivine (Fo 85–87) from P4 and a rare olivine–clinopyroxene nodule from P4 which are suggested to have a genetic link with the precursor melt of the respective intrusions. The third population represents clearly magmatic minerals such as euhedral phenocrysts of Fe-rich olivine (Fo 85–90) crystallised at mantle depths, and olivine overgrowth rims formed contemporaneously with groundmass minerals at crustal levels. Close spatial association and contemporaneous emplacement of P3 kimberlite and P4 lamproite is explained by a unifying petrogenetic model which involves the interaction of a silica-poor carbonatite melt with differently metasomatised wall rocks in the lithospheric mantle. It is proposed that the metasomatised wall rock for lamproite contained abundant MARID-type and phlogopite-rich metasomatic veins, while that for kimberlite was relatively refractory in nature.

Keywords Kimberlite · Lamproite · Olivine · Wajrakarur · India · Xenocrysts

Introduction

Forsteritic olivines characterized by a wide compositional range [Fo = 100 Mg/(Mg + Fe) = 85–94] invariably dominate the macrocryst (0.5–10 mm long) assemblages in kimberlites and olivine lamproites (Clement 1982; Mitchell 1986, 1995; Mitchell and Bergman 1991). Minor element concentrations in olivines, especially those of Ni, Ca, Al, Ti, Mn and Cr have increasingly been found to be useful in the distinction of different olivine populations and of melt-derived from mantle olivines (Howarth and Taylor 2016 and references therein). Olivine cores of zoned macrocrysts from kimberlites and lamproites have varied compositions and can be either xenocrysts derived from disaggregated mantle xenoliths or cognate phenocrysts crystallized from a protokimberlite melt. Multiple textural and/or compositional

Editorial handling: A. Giuliani

Electronic supplementary material The online version of this article (https://doi.org/10.1007/s00710-018-0562-2) contains supplementary material, which is available to authorized users.

✉ Azhar M. Shaikh
azher.shaikh115@gmail.com

[1] EPMA Lab, Department of Earth Sciences, Indian Institute of Technology Bombay, Powai, Mumbai 400076, India

[2] Wadia Institute of Himalayan Geology, Dehra Dun 248 001, India

[3] Geological Survey of India, Bandlaguda, Hyderabad 500068, India

[4] Department of Earth Sciences, Sambalpur University, Burla 768019, India

populations are also known for phlogopites in kimberlites (e.g. Giuliani et al. 2016) and clinopyroxenes in lamproites (e.g. Shaikh et al. 2017). However, little work has been done to correlate different populations of olivine, phlogopite and clinopyroxene within a kimberlite or lamproite in the framework of cognate origin, magmatic origin and inheritance from mantle rocks.

The present study is on two intrusions, P3 and P4, from the Mesoproterozoic Wajrakarur Kimberlite Field (WKF) in southern India, where kimberlites, lamproites and ultramafic lamprophyres are known to occur in close proximity (Shaikh et al. 2017). The classification of many of the WKF intrusions as either kimberlite or lamproite has been a controversial issue primarily because of the lack of detailed mineralogical studies. P3 and P4 have generally been considered as 'kimberlites' based on preliminary mineralogical information (Rao and Phadtre 1966; Akella et al. 1979; Reddy 1987; Scott Smith 1989; Chalapathi Rao et al. 2004). We have undertaken a comprehensive mineralogical study of P3 and P4 rocks in order to: (i) establish their affinity to kimberlite or lamproite; (ii) identify different olivine populations based on their major and minor element compositions obtained from high precision electron microprobe analysis; and (iii) distinguish different populations of phlogopite and clinopyroxene and correlate their paragenesis with that of olivine.

The choice of P3 and P4 for the present study stems from the fact that these are the only intrusions in southern India from where rare mantle-derived ultramafic xenoliths have been reported (Rao and Phadtre 1966; Akella et al. 1979; Reddy 1987) and published major element compositions of olivine in the xenoliths are available (Ganguly and Bhattacharya 1987; Nehru and Reddy 1989) for comparison with our olivine data. Further, P4 is unique in that it contains olivine megacrysts (> 10 mm long), which we analyse along with olivine macrocrysts and examine a possible link between them.

Geological setting

The WKF occurs in the Archaean Dharwar Craton, which is a typical granite–greenstone terrene comprising 3.4–2.7 Ga tonalite–trondhjemite–granodiorite (TTG) gneisses known as the Peninsular Gneisses, volcano-sedimentary schist belts (3.3–2.6 Ga), and granitoid plutons emplaced between 2.6 and 2.5 Ga (Ramakrishnan and Vaidyanadhan 2008). Kimberlites and lamproites are confined to the eastern part of the Dharwar Craton and are distributed in four kimberlite fields and five lamproite fields (compilation in Shaikh et al. 2017). The WKF is the largest field (~ 80 km × 70 km) with 48 intrusions of mainly kimberlites and lamproites and some lamprophyres. Radiometric ages show that the kimberlite and lamproite emplacement peaked around 1100 Ma (Anil Kumar et al. 2007), except for a younger age of ~ 90 Ma for one of the two pulses of TK1 intrusion in WKF (Chalapathi Rao et al. 2016).

P3 (14° 55′ 29″; 77° 17′ 21″) and P4 (14° 55′ 28″; 77° 17′ 49″) are hypabyssal facies intrusions in the Peninsular Gneisses, located ~ 0.8 km apart in the Lattavaram cluster of the WKF (Rao and Phadtre 1966). P3 has a bean-shaped outline with a dimension of 120 m × 40 m, while P4 has an elliptical surface geometry with a dimension of 265 m × 130 m. Both the intrusions are poorly diamondiferous (Ravi et al. 2013).

Samples and analytical techniques

Rock samples for the present study are from a drill core (6 cm diameter) in P3 and from surface outcrops in P4. The numbers of polished thin sections studied include two from P3 and five from P4. Mineral modes of macrocrysts, and microcrysts (0.1–0.5 mm long) were estimated visually by examination of thin sections with a polarising optical microscope, while groundmass mineral proportions were assessed on back-scattered electron (BSE) images using ImageJ software. Quantitative mineral analyses were performed with a five channel WDS CAMECA SX-Five electron probe micro-analyser (EPMA). The details of analytical techniques are described in Supp. Material SM1 and calibration settings of EPMA are given in Supp. Table S1. Modal mineral abundances are presented in Supp. Table S2. EPMA data for olivine, phlogopite, clinopyroxene, spinel, monticellite, K-richterite, perovskite and apatite are given in Supp. Tables S3–S9.

Results

Petrography

P3 and P4 samples are inequigranular textured rocks with significant mineralogical differences between them. Based on microtextural and compositional characteristics, multiple populations of olivine, phlogopite and clinopyroxene are recognised in both P3 and P4. These populations are designated as I, II and III with the third population being subdivided into IIIa, IIIb and IIIc. Olivine commonly shows secondary alteration which is more pronounced in P3 compared to P4.

P3 rock

P3 samples are characterized by macro- and microcrysts of olivine and phlogopite set in a groundmass dominated by

phlogopite and monticellite with subordinate amounts of serpentine, spinel, perovskite, apatite, calcite and rare baddeleyite (Supp. Fig. 1a–f). Spinel grains commonly show atoll texture. Although olivine crystals are usually highly serpentinised, a core-rim structure can be identified in some of the macrocrysts in back-scattered electron (BSE) images. Mg-rich cores of olivine macrocrysts which are relatively dark compared to the rims in BSE images are designated as olivine-I. Fe-rich cores of zoned olivine macrocrysts which are relatively bright compared to the rims in BSE images are classified as olivine-II. Some olivine-II macrocrysts contain rare inclusions of ilmenite (Supp. Fig. 1a). Overgrowth rims on olivine-I and olivine-II cores, and rare olivine inclusions in monticellite (Supp. Fig. 1b) are designated as olivine-III.

Phlogopites of three populations are distinguished. Phlogopite-I includes: (i) glimmerite nodules (Supp. Fig. 1c); (ii) phlogopite–clinopyroxene nodules; and (iii) discrete macrocrysts (up to 1.4 mm long) locally showing intergrowth with vermicular spinel (Supp. Fig. 1d). Phlogopite II forms: (i) lining along intergranular boundaries in glimmerite nodules of phlogopite-I (Supp. Fig. 1c); (ii) overgrowth on the phlogopite-I core of macrocrysts (Supp. Fig. 1e); and (iii) discrete microcrysts. Crystals of both phlogopite-I and phlogopite-II are often deformed into a bent shape and also show resorption, which has resulted in a rounded shape or corroded grain boundary (Supp. Fig. 1d, e). Glimmerite nodules also have a resorbed outline (Supp. Fig. 1c). Phlogopite-III population modally dominates over other types of phlogopite and occurs as: (i) poikilitic laths in the groundmass containing inclusions of spinel, perovskite and apatite (Supp. Fig. 1f); (ii) aggregates in groundmass segregations; and (iii) numerous tiny needles (< 50 µm long) scattered throughout the groundmass and also as filling material in some of the pseudomorphs after olivine.

Clinopyroxene grains constituting the phlogopite–clinopyroxene nodules mentioned above are classified as clinopyroxene-I. Highly corroded and sieve-textured discrete macrocrysts of clinopyroxene are also included in this population.

P4 rock

P4 samples are marked by mega-, macro- and microcrysts of olivine and microphenocrysts of clinopyroxene set in a groundmass dominated by clinopyroxene and phlogopite with subordinate amounts of serpentine, spinel, perovskite, apatite, and occasional gittinsite. Three populations of olivine are identified (Fig. 1a–f). Olivine-I macrocrysts are anhedral to sub-rounded and sometimes contain inclusions of other peridotitic minerals such as spinel (Fig. 1a) and orthopyroxene. Some of the olivine-I macrocrysts display evidences of plastic deformation such as undulose extinction and deformation band, while recrystallisation (Passchier and Trouw 2005) in parts of the crystals has resulted in the development of a mosaic texture (Arndt et al. 2010) (Fig. 1b) and neoblasts or tablets (Brett et al. 2009; Arndt et al. 2010) (Fig. 2e, f). Neoblasts have a different optical orientation than that of the host olivine (Fig. 2e).

The olivine-II population comprises discrete macrocrysts and megacrysts, and constituent grains in a rare olivine–clinopyroxene nodule (Fig. 2a, b). The nodule (~ 2 mm diameter) shows spongy patches marked by small inclusions of olivine and spinel (< 30 µm long) in the marginal part of clinopyroxene grains. Olivine-III includes three sub-groups designated as IIIa, IIIb and IIIc. Olivine-IIIa represents symmetrical euhedral phenocrysts and microphenocrysts that are elongate to equant in shape (Fig. 1e, f) and contain rare inclusions of groundmass spinel. Elongate phenocrysts of olivine-IIIa are up to 1.5 mm long and have aspect ratios of up to 4.7:1 (Fig. 1e). Some of these phenocrysts are deformed into a bent shape (Fig. 4c). Olivine-IIIb includes overgrowth rims which are up to 200 µm wide and mantle either olivine-I (Fig. 1a) or olivine-II (Fig. 4b) core and locally contain inclusions of groundmass phases like phlogopite, perovskite and spinel. Olivine-IIIc comprises irregular and patchy alteration zones developed adjacent to intragranular fractures (Fig. 1b) and at the rims (Fig. 1d) of olivine-I macrocrysts and along grain boundaries of olivine-I neoblasts (Fig. 1c).

Phlogopite-I and phlogopite-II identified in P3 have not been found in P4 samples. Phlogopite-III in P4 includes poikilitic laths of phlogopite containing inclusions of other groundmass minerals such as perovskite, spinel and clinopyroxene (Fig. 2d). Clinopyroxene-I is absent in P4 samples. Clinopyroxene occurring in association with olivine-II in the olivine–clinopyroxene nodule (Fig. 2a, b) in P4 is designated as clinopyroxene-II. Clinopyroxene-II also occurs as inclusions in olivine-II megacrysts. K-richterite is a rare phase in P4 occurring along with clinopyroxene-II at the boundary between the olivine-I core and olivine-IIIb overgrowth rim (Fig. 2c). Clinopyroxene-III forms microphenocrysts, and scattered crystals and radiating aggregates in the P4 groundmass.

Mineral chemistry

Olivine

The ranges of Fo content and Ni, Ca, Mn, Ti, Al, Cr, Na and Co concentrations for different olivine populations from P3 and P4 are presented in Table 1. Complete analyses of olivines are given in the Supp. Table S3.

P3 olivines Olivine-I macrocrysts are marked by higher contents of Fo (90–93) and Ni relative to olivine-II crystals, but lower concentrations of Ca, Co and Mn (Table 1). Further,

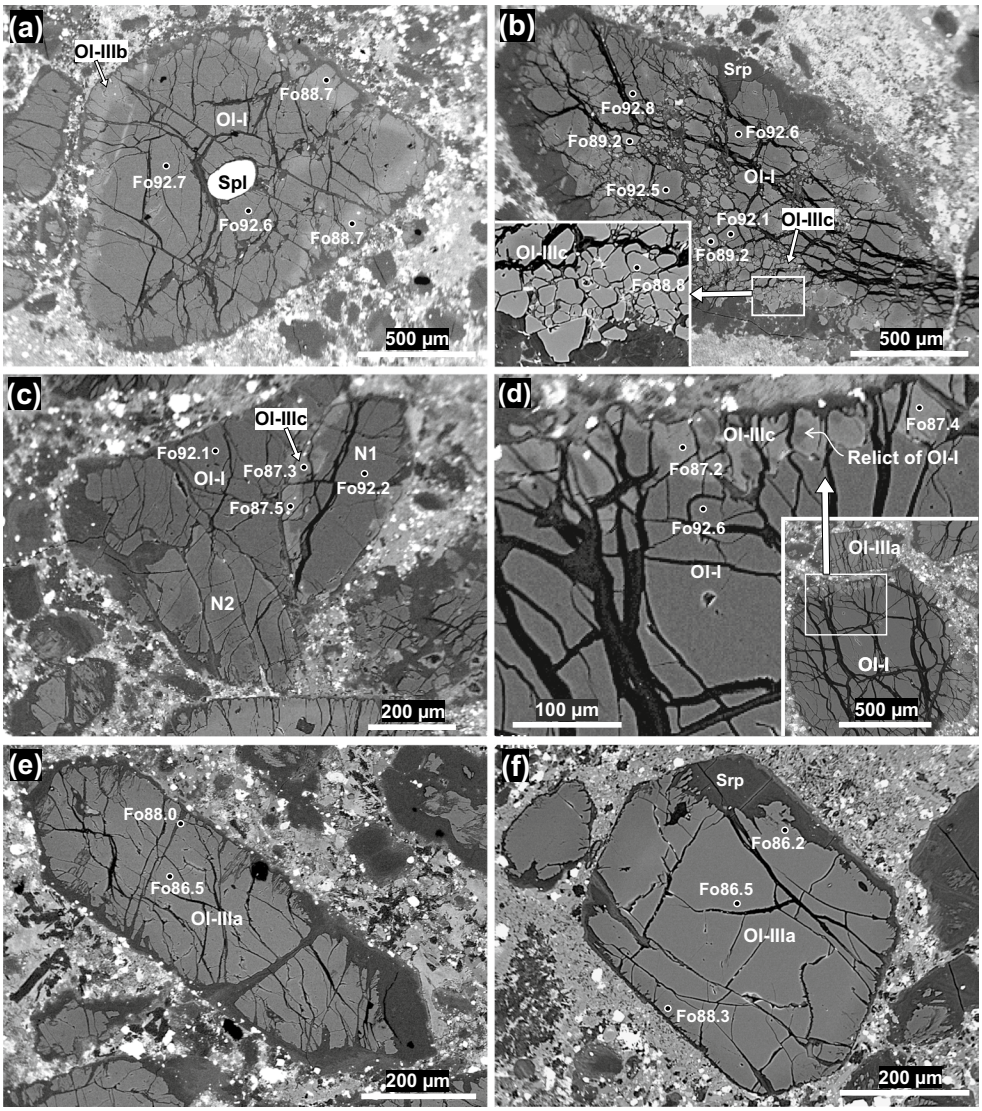

Fig. 1 Olivine textures in P4 samples. **a** to **f** are back scattered electron images in which brighter shades represent relatively Fe-rich compositions. **a** Normal-zoned macrocryst with olivine-I core and overgrowth rim of olivine-IIIb. **b** Olivine-I macrocryst showing partial recrystallisation in the southern part to a fine-grained mosaic texture, and alteration zones olivine-IIIc adjacent to intragranular fractures. **c** Neoblasts (N1 and N2) developed from olivine-I macrocryst; N1 shows partial alteration to olivine-IIIc at the grain boundary, while N2 is altered for the most part to olivine-IIIc. **d** Olivine-IIIc alteration rim with relict islands of Fo-rich olivine; inset shows the parent olivine-I macrocryst. **e** Elongate phenocryst of olivine-IIIa. **f** Equant phenocryst of olivine-IIIa. The phenocrysts lack in discrete overgrowth but show higher Fo content towards the rim

the olivine-I population is clearly differentiated from olivine-II and olivine-III populations on the plots of Ni vs Ca (Fig. 3c) and Ni vs Mn (Fig. 3e). Olivine-II macrocrysts form a decreasing trend of Fo (89–81) and NiO (Fig. 3a).

Olivine-III overgrowth rims have moderate Fo contents (Fig. 3a), except for the single olivine inclusion in monticellite (Supp. Fig. 1b) which is exceptionally rich in Mg with Fo 96. These rims are marked by higher Ca, Mn, Ti, Al and Cr, and lower Ni contents compared to olivine-I. A line profile of a reverse-zoned (Fe-rich core) macrocryst from P3 shows that it has an olivine-II core of fairly uniform composition, while the overgrowth rim is marked by almost constant Fo content, but decreasing Ni, increasing Mn and fluctuating Ca and Cr from the inner margin to the outer margin of the rim (Fig. 4a). The plot of NiO vs Fo also clearly shows a decreasing trend of NiO at nearly constant Fo (Fig. 3a). The olivine-III inclusion in monticellite has the highest concentrations of Ca and Mn among the P3 olivines.

P4 olivines P4 olivine-I macrocrysts have similar Fo contents (91–93) and Ni, Ca, Co and Mn concentrations as those from P3 (Table 1 and Fig. 3b, d, f). Olivine-II macrocrysts

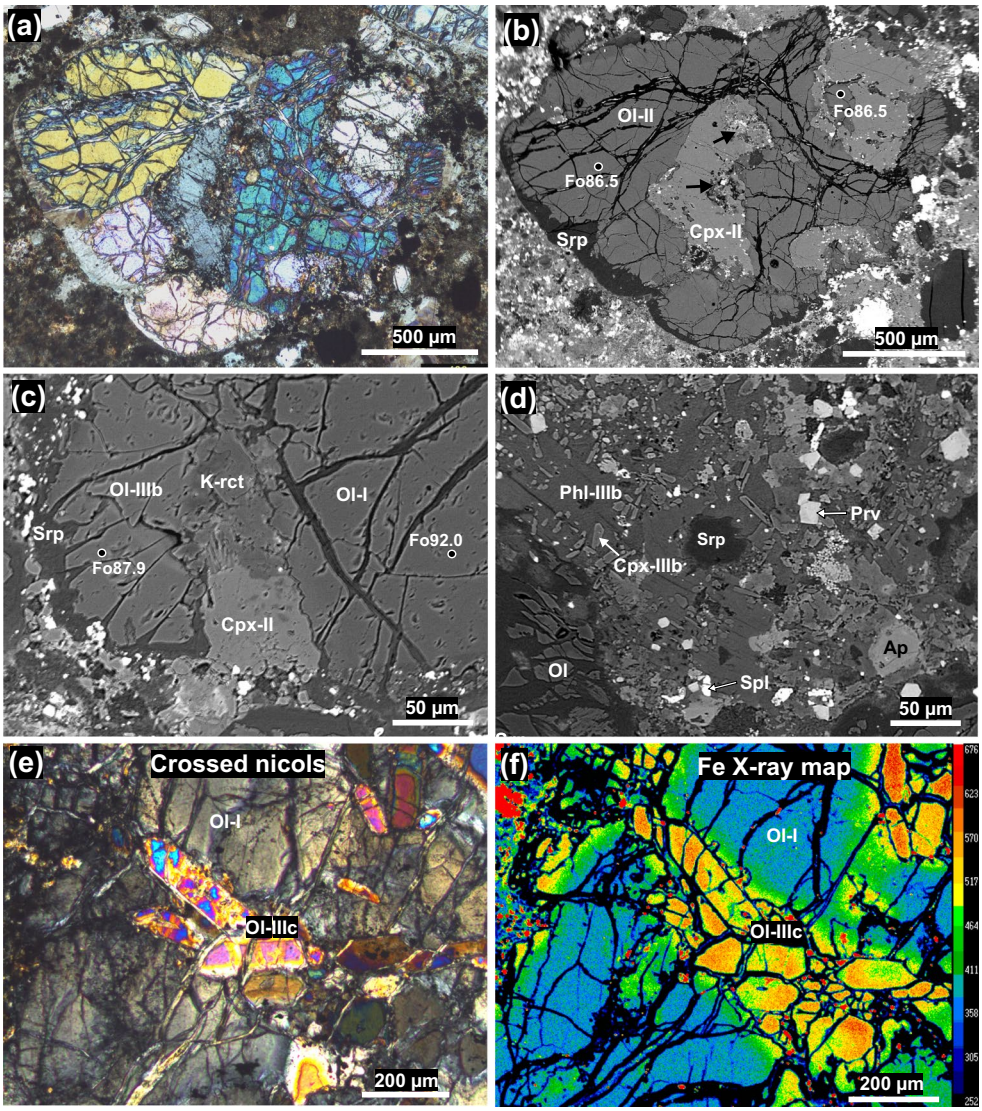

Fig. 2 Photomicrograph (**a**) and back scattered electron images (**b**–**f**) of P4 samples. Fo content in olivine is shown at representative spots. **a** Olivine–clinopyroxene nodule of type-II minerals in crossed nicols showing different olivine grains marked by distinct interference colours. **b** BSE image of the same nodule as (**a**) showing spongy areas marked by black arrows in the marginal part of clinopyroxene grain. **c** K-richterite and clinopyroxene-II occurring at the interface of olivine-I core and olivine-IIIb overgrowth rim. **d** Poikilitic laths of phlogopite-IIIb in the groundmass containing inclusions of perovskite, spinel and clinopyroxene-IIIb. **e** Photomicrograph of a part of an olivine-I macrocryst; crystals with bright interference colours are neoblasts with different optical orientations than the host olivine. **f** Fe X-ray map of the same area as (**e**) showing Fe-rich alteration zones of olivine-IIIc adjacent to intragranular fractures

and megacrysts from P4 have relatively low Fo contents which mostly fall in a narrow range of 85–87 and overlap with the field of megacrysts from worldwide kimberlites (Gurney et al. 1979; Hops et al. 1992). The olivine-II crystals have a restricted range of Fo and higher concentrations of Ni and Cr compared to those from P3.

Crystals and rims of the three subgroups of olivine-III have Fe-rich composition. Olivine-IIIa phenocrysts span a wide range of Fo content (85–90), while olivine-IIIb overgrowth rims and olivine-IIIc alteration rims have a rather restricted range of Fo87–90. The three subgroups show marked differences in their minor element distribution (Fig. 3b, d, f). Olivine-IIIa phenocrysts have high Ni and low Ca contents falling within relatively restricted ranges compared to olivine-IIIb overgrowth rims, which exhibit large variations in these elements. A comparison of overgrowth rims from P3 and P4 shows that the latter are marked by higher values of Ca, Ti, Al and Cr. Further, the P4 overgrowth rims show an overall decrease of NiO with Fo (Fig. 3b).

Three olivine crystals have been chosen for the illustration of zoning patterns: (i) reverse-zoned (Fe-rich core)

Table 1 Ranges of forsterite molar fractions and trace element concentrations for different olivine populations from intrusions P3 and P4

Element	Intrusion	Olivine-I macrocrysts	Olivine-II macrocrysts	Olivine-II megacrysts	Olivine-IIIa phenocrysts	Olivine-IIIb overgrowth rims	Olivine-IIIb inclusion in monticellite	Olivine-IIIc M1 alteration	Olivine-IIIc M2 alteration
Forsterite fraction (mol%)									
	P3	90–93	81–89	n.o	n.o	88–89	96	n.o	n.o
	P4	91–93	85–87 (one at 83)	86–87	85–90	87–90	n.o	88–90	87–89
Trace elements (ppm)									
Ni	P3	2344–2793	1046–2387	n.o	n.o	1132–2206	621	n.o	n.o
	P4	2084–3192	1709–2648	2377–2469	2085–3168	256–2914	n.o	2292–3045	1526–2589
Ca	P3	100–308	250–599	n.o	n.o	306–532	3459	n.o	n.o
	P4	107–357	226–748	498–645	515–1005	252–2443	n.o	334–976	3753–4417
Mn	P3	632–853 (few up to 1107)	870–1416	n.o	n.o	853–1195	2231	n.o	n.o
	P4	566–856	961–1247	947–997	849–1172	800–1415	n.o	800–1154	3446–4361
Ti	P3	bdl–108	75–148	n.o	n.o	138–179	n.a	n.o	n.o
	P4	bdl–124	70–162	182–217	86–221	63–308	n.o	72–199	bdl–43
Al	P3	bdl–80	bdl–264	n.o	n.o	60–151	n.a	n.o	n.o
	P4	35–137	17–217	62–197	104–703	49–418	n.o	76–170	bdl–19
Cr	P3	142–291	34–297	n.o	n.o	180–397	n.a	n.o	n.o
	P4	67–588	123–743	392–605	115–932	171–1036	n.o	116–760	33–139
Na	P3	64–119	53–197	n.o	n.o	60–202	n.a	n.o	n.o
	P4	47–185	76–205	170–270	108–264	50–221	n.o	98–236	53–103
Co	P3	131–174	181–266	n.o	n.o	155–215	n.a	n.o	n.o
	P4	139–196	196–264	223–252	185–274	172–233	n.o	169–242	206–250

bdl below detection limit, *n.a.* not analysed, *n.o.* not observed

macrocryst with a uniform core of olivine-II and overgrowth rim of olivine-IIIb; (ii) reverse-zoned phenocryst with a zoned core of olivine-IIIa and overgrowth rim of olivine-IIIb; and (iii) normal-zoned macrocryst with a uniform core of olivine-I and overgrowth rim of olivine-IIIb (Fig. 4b, c, d). Identification of overgrowth zoning on olivine-IIIa phenocrysts is not straightforward because the phenocrysts may originally be zoned during growth. This is exemplified in the Fig. 4c, where a smoothly increasing trend of Fo content in the phenocryst continues unchanged from the core to the rim. But the existence of an overgrowth rim is detected from the sharp increase in Ca and Mn and steep fall in Ni and Cr in the outermost part of the rim.

Olivine-IIIc alteration rims (Fig. 1d) have clearly resulted from solid–melt interaction, the effect of which is also evident from numerous alteration zones adjacent to intragranular fractures where the Fo content is appreciably lower than that of the parent olivine-I (Fig. 1b). Mosaic textured parts (Fig. 1b) and neoblasts (Fig. 1c) developed from recrystallised olivine-I macrocrysts exhibit varying degrees of alteration to Fe-rich compositions. Altered neoblasts sometimes show a zoning pattern of increasing Fe (Fig. 2f) and Ca and decreasing Mg from the core to the rim with Ni remaining uniform. The Mg-rich core of the neoblasts is reminiscent of the parent higher Fo olivine-I, while Fe and Ca have increased due to solid–melt interaction. Such neoblast zoning contrasts with the olivine-IIIa phenocryst zoning, where Mg increases from the core to the rim (Fig. 4c). The alteration rims and zones interestingly show two distinct compositional trends, designated as M1 and M2. The Ni content of the M1 alteration trend is broadly similar to that of the parent olivine-I macrocrysts, while M2 alteration trend has somewhat lower Ni content (Fig. 3b). The M2 is marked, relative to M1, by a sharp increase in Ca and Mn and low Ti, Al, Cr and Na. However, the Ca and Mn concentrations in both M1 and M2 trends are higher than those of the parent olivine-I.

Phlogopite

The three phlogopite populations I, II and III from P3 have X_{Mg} ($=Mg/Mg+Fe^{T}$) in the range of 0.85–0.96 (Supp. Table S4). The mica populations can be distinguished in terms of their Cr_2O_3, TiO_2, Al_2O_3, BaO and F contents. Phlogopite-I micas are characterized by high Cr–low Ti–low Ba composition with 0.1–1.3 wt% Cr_2O_3, 0.2–1.7 wt% TiO_2 and < 0.5 wt% BaO, and are tightly constrained with respect

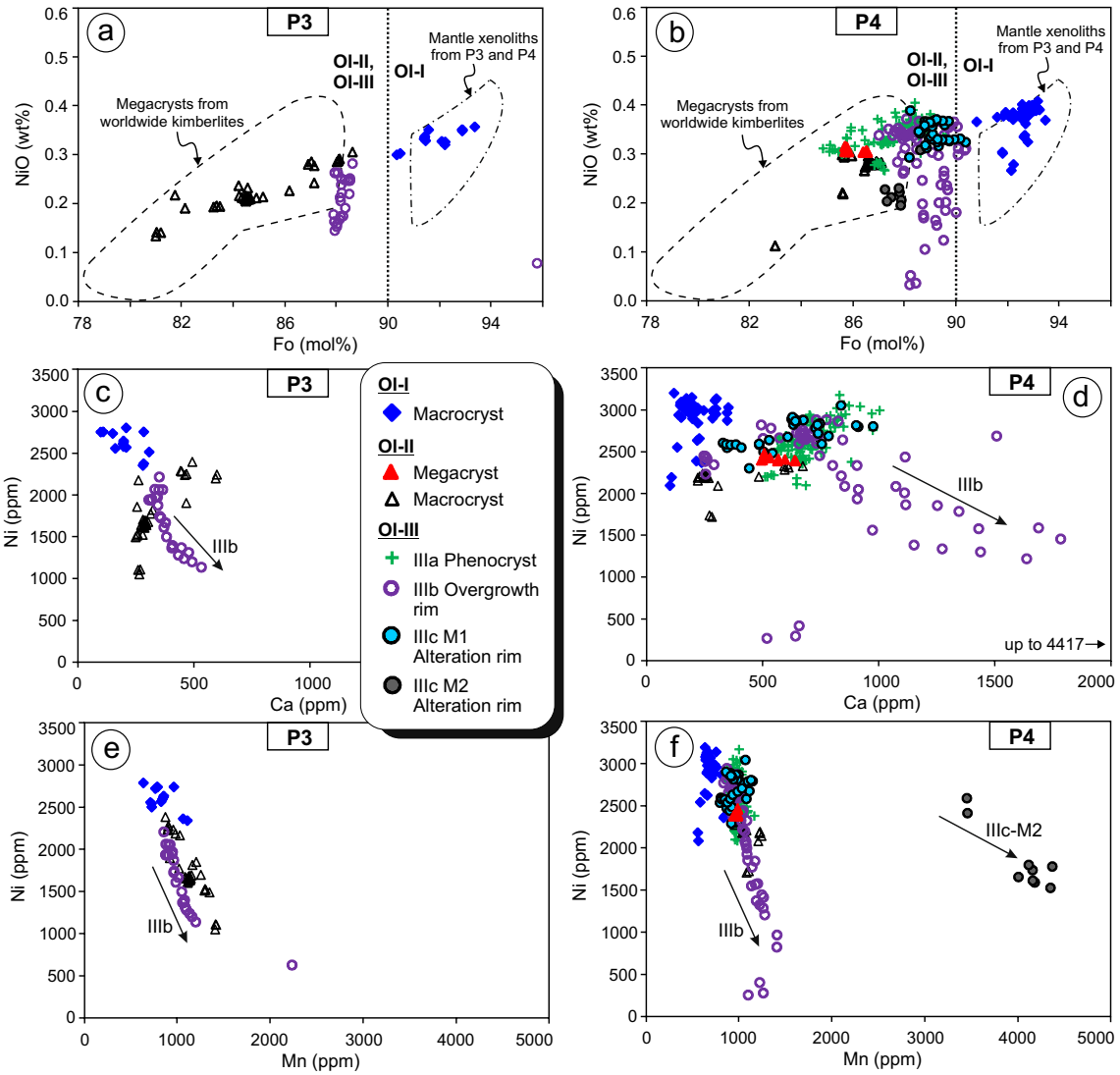

Fig. 3 Compositional plots for olivines from P3 and P4. NiO (wt%) vs Fo content (**a, b**); field for mantle xenoliths is from the data of Ganguly and Bhattacharya (1987) and Nehru and Reddy (1989); the field for megacrysts from worldwide kimberlites is after Lim et al. (2018). Plots of concentration (in ppm) of Ni against Ca (**c, d**), and Mn (**e, f**). Note the distinct clusters for olivine-I macrocrysts

to their Al_2O_3 content (11.3–13.0 wt%). These phlogopites exhibit a broadly positive correlation of Cr_2O_3 and NiO with X_{Mg}. Phlogopite-II micas are of high Cr–high Ti–moderate Ba type with 0.3–1.1 wt% Cr_2O_3, 3.8–5.8 wt% TiO_2, 0.1–2.5 wt% BaO and exhibit a wide range of Al_2O_3 content (12.3–17.4 wt%). Phlogopite-III micas are marked by low Cr–low Ti–high Ba composition with < 0.2 wt% Cr_2O_3, < 1 wt% TiO_2 and up to 6.2 wt% BaO. These micas show a wide range of Al_2O_3 content (9.3–16.7 wt%) and their fluorine content is usually high (up to 3.3 wt% F). In the Al_2O_3 vs FeO^T and Al_2O_3 vs TiO_2 plots phlogopite-III micas follow the Al-enrichment trend without significant variation in FeO^T and TiO_2 (Fig. 5a, b).

The single mica population of phlogopite-III from P4 has X_{Mg} in the range of 0.72–0.90 (Supp. Table S4). The phlogopites are of low Cr–moderate Ti–moderate Ba type with < 0.2 wt% Cr_2O_3, up to 3.5 wt% TiO_2 and up to 4.9 wt% BaO. Their Al content is usually low (2.9–12.1 wt% Al_2O_3), which is compensated by tetraferric iron (0.045–0.976 cations per 22 oxygen). Fluorine content of P4 phlogopites (0–5.0 wt% F) is in most cases higher than that from P3 (0–3.3 wt% F). P4 phlogopites show a trend of Al-depletion with increasing FeO^T and either increasing or nearly constant TiO_2 (Fig. 5a, b).

Pyroxene

Clinopyroxene-I occurring in phlogopite–clinopyroxene nodules from P3 is diopside to augite in composition

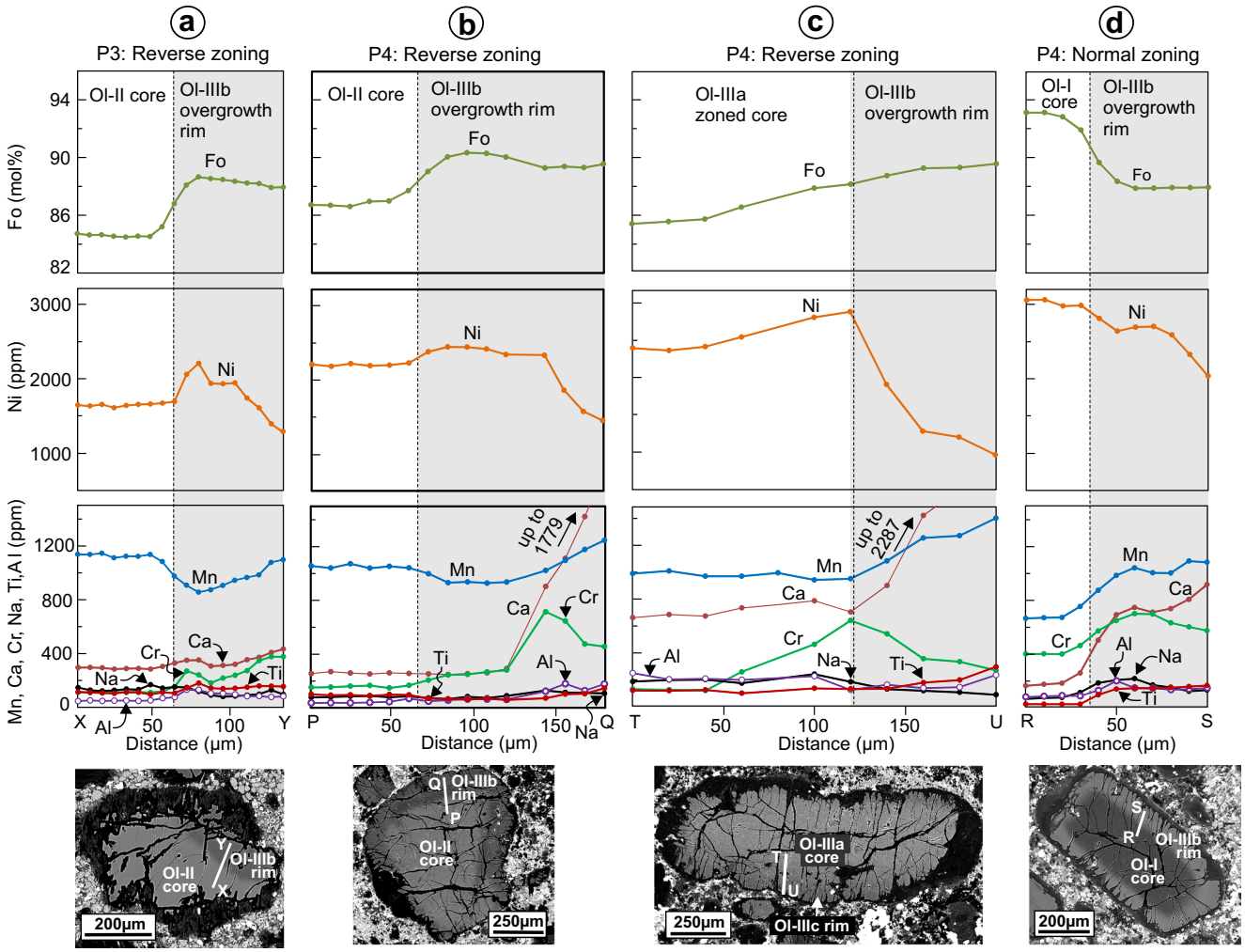

Fig. 4 BSE images and core to rim profiles of forsterite content and concentrations of Ni, Mn, Ca, Cr, Al, Ti and Na in olivine. Reverse-zoned crystals from P3 (**a**) and P4 (**b, c**), and normal-zoned crystal from P4 (**d**). The crystal in (**c**) is a bent phenocryst of olivine-IIIa showing primary growth zoning, mantled by an overgrowth zone of olivine-IIIb

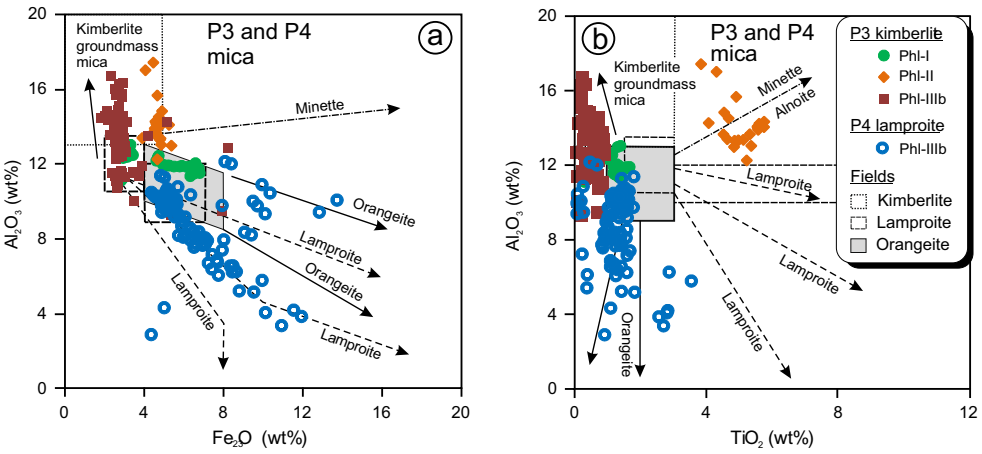

Fig. 5 Al_2O_3 vs FeO^T (**a**) and Al_2O_3 vs TiO_2 (**b**) plots for mica from P3 and P4 intrusions; fields and trends of kimberlites, orangeites and lamproites are after Mitchell (1995)

with moderate values of Cr_2O_3 (0.3–1.5 wt%) and Al_2O_3 (0.7–2.0 wt%), and low TiO_2 (< 1.1 wt%) (Supp. Table S5).

Clinopyroxene-II occurring in olivine–clinopyroxene nodule from P4 is also diopside to augite in composition with low TiO_2 (0.2–0.6 wt%) and moderate Al_2O_3 (0.3–2.1 wt%) contents, but has increased values of Cr_2O_3 (1.4–2.0 wt%). Clinopyroxene-III crystals from P4 are diopside to augite with X_{Mg} (= Mg/Mg + Fe) values varying widely from 0.53 to 0.93. Although they have low contents of Cr_2O_3 (< 0.2 wt%) and Al_2O_3 (< 1.0 wt%), their TiO_2 content reaches high values (up to 3.5 wt%), which is typical of lamproitic clinopyroxenes (Mitchell and Bergman 1991). In the Ti vs Al plot, the P4 clinopyroxene-III compositions fall in the field of worldwide lamproites and orangeites (Supp. Fig. 2a).

Spinel

P3 spinels show extensive variation in composition from titanian (3.2–11.1 wt% TiO_2), aluminous (5.7–13.2 wt% Al_2O_3) magnesiochromite (24.1–52.5 wt% Cr_2O_3), to Mg-free or magnesian (0–11.1 wt% MgO) Ti-free or titanian (0–3.1 wt% TiO_2) magnetite (Supp. Table S6). In the oxidized spinel prism, P3 spinels show the magnesian ulvospinel trend (trend 1) of Mitchell (1986) (Fig. 6a).

P4 spinels show compositional variation from titanian aluminous magnesiochromite through titanian magnesiochromite (1.4–7.3 wt% TiO_2; 2.2–17.5 wt%; 20.1–59.9 wt% Cr_2O_3) to Ti-magnetite (1.8–5.8 wt% MgO; 0–10.1 wt% TiO_2). In the oxidized spinel prism, P4 spinels show the typical Fe-Ti enrichment trend also known as titanomagnetite trend (trend 2) of Mitchell (1986) (Fig. 6b). A few grains of highly Al-rich spinels (27.5–48.2 wt% Al_2O_3) with low X_{Fe} (0.18–0.41) form a distinct cluster near the base of the spinel prism. The spinel inclusion in the olivine-I macrocryst from P4 (Fig. 1a) is an aluminous magnesiochromite with 59.3 wt% Cr_2O_3, 12.7 wt% MgO, 6.8 wt% Al_2O_3, which is compositionally similar to spinels in lherzolite xenoliths from P3 (Nehru and Reddy 1989).

Other minerals

P3 monticellite, perovskite and apatite Monticellites have Mg# in the range of 0.89–0.95 and fall in the field for global kimberlites in the Mg_2SiO_4–$CaMgSiO_4$–$CaFeSiO_4$ ternary plot (Supp. Table S7; Supp. Fig. 2b) and are, therefore, diagnostic of kimberlite affinity. Perovskite grains are commonly zoned with the core enriched in $\sum LREE_2O_3$ (up to 4.0 wt%) and Nb_2O_3 (1.1–1.9 wt%) relative to the rim (1.0–2.1 wt% $\sum LREE_2O_3$ and < 1.3 wt% Nb_2O_3) (Supp. Table S8). SrO content of perovskites is generally low with values mostly below 0.5 wt% in common with other kimberlite perovskites (Mitchell 1986, 1995). Two generations of apatite are found. Early formed prismatic crystals are relatively enriched in F (2.5–5.1 wt%) and depleted in SrO (< 2.0 wt%) and BaO (< 0.05 wt%), while the late formed amoeboid-shaped apatites are F-poor (< 1.8 wt%), but highly enriched in SrO (2.0–13.6 wt%) with minor amount of BaO (< 0.5 wt%) (Supp. Table S9).

P4 K-richterite, perovskite and apatite K-richterite has low Al_2O_3 (0.2–1.6 wt%) content (Supp. Table S7) typical of most lamproite amphiboles (Mitchell and Bergman 1991). In terms of FeO (1.6–3.4 wt%), TiO_2 (0.1–0.8 wt%) and F (2.6–3.9 wt%) contents and Na/K ratios (1.4–2.3), it is comparable to TK4 lamproite amphibole from the WKF (Shaikh et al. 2017). Perovskite grains are broadly homogeneous with 0.2–3.3 $\sum LREE_2O_3$ and 0.4–1.1 wt% Nb_2O_3. They contain significant levels of SrO (up to 1.3 wt%) which is similar to most lamproite perovskites (Mitchell and Bergman 1991). Apatites are of two generations. Early-formed apatite crystals have high F (2.6–4.9 wt%) and low SrO (< 2 wt%) contents. Late generation apatites, which mantle

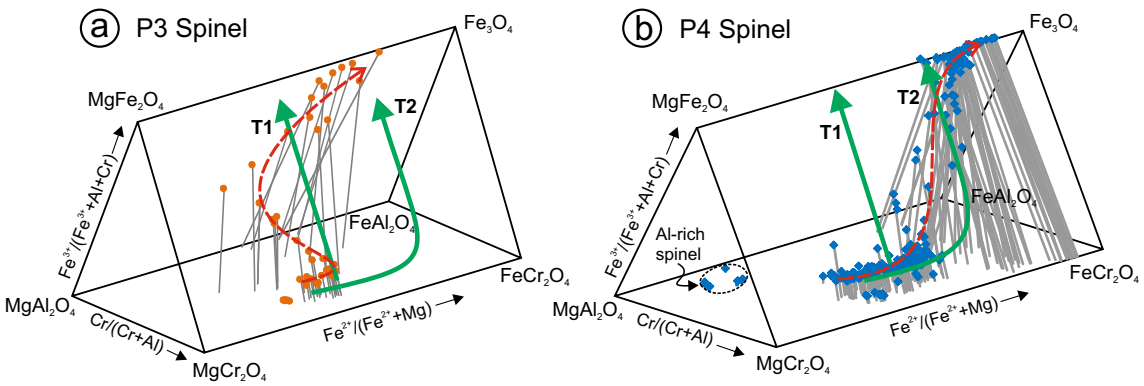

Fig. 6 Oxidized spinel prism plots showing magnesian ulvospinel trend (T1) of P3 spinels (**a**) and titanomagnetite trend (T2) of P4 spinels (**b**); trends T1 and T2 are after Mitchell (1986)

these crystals, are marked by relatively low F (1.3–3.1 wt%) and high SrO (4.0–8.8 wt%) contents. A notable feature of the apatites is their high BaO content (1.4–5.3 wt%) in the late generation which is similar to those reported in many lamproites, especially from Prairie Creek and Walgidee Hills (Mitchell and Bergman 1991).

Discussion

Classification

P3 is considered as archetypal kimberlite based on the following groundmass mineralogical data: (i) the groundmass is dominated by phlogopite and monticellite; (ii) phlogopite micas show the characteristic Al-enrichment trend without significant variation in FeO^T and TiO_2 (Mitchell 1986, 1995); (iii) spinels, commonly with atoll texture, exhibit the magmatic trend 1 in spinel prism; and (iv) monticellite crystals have composition similar to that of global kimberlites. While P3 was classified as monticellite kimberlite by Scott Smith (1989), and phlogopite kimberlite by Chalapathi Rao et al. (2004), our observation shows that phlogopite is equally dominant as monticellite in the groundmass. Hence, P3 should rather be classified as phlogopite–monticellite kimberlite.

Scott Smith (1989) classified P4 as mica-bearing monticellite kimberlite, while Chalapathi Rao et al. (2004) described P4 as phlogopite kimberlite. However, our mineralogical data are at variance with these classifications. The following observations on the groundmass mineralogy indicate affinity of P4 towards lamproite: (i) the groundmass is dominated by Al-poor diopside and phlogopite; (ii) phlogopite micas show the characteristic trend of Al-depletion with increasing FeO^T and either increasing or nearly constant TiO_2 (Mitchell and Bergman 1991); (iii) elevated F content of the micas; (iv) spinels exhibit the magmatic trend 2 in spinel prism; (v) Ba-rich composition of fluorapatites; and (vi) elevated SrO content of perovskites. Although some of these mineralogical characteristics are also common in orangeites (Mitchell 1995) and there is a lack of typomorphic minerals such as leucite, sanidine, priderite and wadeite, P4 can be classified as an olivine lamproite of unusual composition because; (i) several WKF intrusions (P2-west, P5, 12, P13) with similar mineralogical characteristics as P4 have been classified as unusual lamproites (Gurmeet Kaur et al. 2013; Gurmeet Kaur and Mitchell 2013, 2016); (ii) K-richterite, though rare in P4, has similar composition as amphibole from TK4 lamproite (Shaikh et al. 2017); and (iii) absence of carbonate in P4 which is an essential constituent of most orangeites (Mitchell 1995).

Origin of olivine, clinopyroxene and phlogopite of different generations

Type I crystals and nodules

Mg-rich olivine-I macrocrysts from both P3 and P4 are considered to be disaggregated peridotite xenoliths because: (i) their compositions with high Fo content and Ni and low Ca, Co and Mn are typical of xenocrystic olivine cores from kimberlites and lamproites worldwide (e.g. Giuliani et al. 2017; Shaikh et al. 2017 and references therein); (ii) on the plot of NiO vs Fo content, their compositions lie within the field of olivines from mantle-derived xenoliths of lherzolite, harzburgite and dunite from P3 and P4 (Ganguly and Bhattacharya 1987; Nehru and Reddy 1989); (iii) they contain inclusions of other peridotitic minerals such as orthopyroxene and magnesiochromite with compositions similar to these minerals in lherzolite and harzburgite xenoliths from P3 and P4; and (iv) they exhibit plastic deformation in the form of undulose extinction and deformation bands which are common features of xenocrystic olivine (Mitchell 1986).

Microtextural attributes of clinopyroxene-I from P3 such as its relict nature in phlogopite–clinopyroxene nodules and corroded shape of discrete macrocrysts suggest that the mineral was out of equilibrium with the P3 kimberlite melt. Phlogopite-I micas occurring in phlogopite–clinopyroxene and glimmerite nodules, and as discrete macrocrysts in P3 are all characterised by similar concentration levels of Cr and Ti that are comparable with those of phlogopite cores in mantle xenoliths from several South African kimberlites (e.g. Carswell 1975; Dawson and Smith 1975; Giuliani et al. 2016). Vermicular spinel, intergrown with phlogopite-I macrocrysts from P3, is known to occur in peridotite nodules from the Kimberly pipes, South Africa (Erlank et al. 1987). These textural and compositional aspects taken together indicate that the macrocrysts of phlogopite-I and clinopyroxene-I are derived from disaggregation of the mantle xenoliths. Highly Al-rich spinels from P4 which form a distinct cluster near the base of the spinel prism are also considered to be mantle-derived xenocrysts.

Type II crystals and nodules

P3 samples contain olivine and phlogopite as Type II minerals and are marked by the characteristic absence of clinopyroxene. Phlogopite-II micas from P3 are interpreted to have crystallised at mantle depths based on their elevated chrome content (Lloyd et al. 2002; Giuliani et al. 2016). These phlogopites record plastic deformation, which probably occurred during their transport in the ascending magma.

In P4, Fe-rich olivine-II macrocrysts, megacrysts and constituent grains in the olivine–clinopyroxene nodule have overlapping major and minor element compositions. Further,

clinopyroxene inclusions in olivine-II megacrysts are compositionally similar to the clinopyroxene grains in the nodule. These attributes suggest that the olivine-II macrocrysts and megacrysts and olivine–clinopyroxene nodule are all genetically related.

The origin of Fe-rich olivines is a matter of debate and two options are generally invoked for their origin. These are considered either as xenocrysts of mantle material unrelated to kimberlite or lamproite development (Bussweiler et al. 2015) or as cognate phenocrysts genetically related to a precursor melt in the early stage of kimberlite or lamproite magmatism (e.g. Kopylova et al. 2009; Kamenetsky et al. 2014; Howarth and Taylor 2016). Support for the latter comes from geochronological studies of megacryst suites from kimberlites which have documented the same age for the megacrysts and their host intrusion (Kopylova et al. 2009; Tappe et al. 2011; Kamenetsky et al. 2014). In the case of P3 and P4, the Fo content and minor element compositions of olivine-II population overlap with those of the magmatic olivine-III population which suggest a genetic link of the former to a precursor melt of kimberlite in P3 and of lamproite in P4.

While a genetic link is apparent between the type II crystals (including megacrysts) and precursor melts, the exact processes which resulted in this link remain unconstrained. Several studies on megacryst suites, mainly from kimberlites, suggest their crystallisation from precursor melts, metasomatism and interaction with wall rocks as megacryst-forming processes (e.g. Gurney et al. 1979; Kopylova et al. 2009; Giuliani et al. 2013; Moore and Costin 2016; Kargin et al. 2017). In the present study, the spongy texture in the olivine–clinopyroxene nodule from P4 indicates lack of recrystallisation and prolonged annealing, which in turn suggests an origin by metasomatism (Su et al. 2011). However, whether the metasomatism occurred immediately prior to the magmatic eruption or during transport by the host magma is unknown. In P3 kimberlite, olivine-II macrocrysts show a wide range of Fo content with the most Fe-enriched at Fo81 which is consistent with their formation along with phlogopite (Lim et al. 2018). Such Fe-rich composition and a positive Fo–NiO correlation are analogous to those of kimberlitic megacrysts (Gurney et al. 1979; Hops et al. 1992).

Olivine-IIIa phenocrysts: high pressure crystallisation

Plastic deformation of olivine-IIIa phenocrysts indicates that the crystals were subjected to plastic deformation during emplacement which is different from the late-stage (crustal level) olivine deformation manifested in the form of brittle fractures traversing the crystals. It is reasonable to believe that the phenocrysts crystallised at mantle depths under high pressure–temperature conditions and were subsequently emplaced in a plastic or near solid state so that they could be deformed by torsional forces applied to the magma during intrusion (Kreston 1973). Skinner (1989) envisaged crystallisation of olivine phenocrysts at mantle depths from small discrete melt pockets before the magma's ascent. Kamenetsky et al. (2008) calculated pressure–temperature conditions of 45–50 kbar and 900–1000 °C for high pressure crystallisation of olivine (olivine-II cores in their nomenclature) from the Udachnaya-East kimberlite. In order to preclude very high speeds of magma's ascent at this stage, Kamenetsky et al. (2008) suggested loading of the magma with a large amount of solid materials so that the magma is sufficiently viscous and dense. Veter et al. (2017) proposed crystallisation of reverse-zoned olivine phenocrysts in Aillik Bay aillikites from earlier batches of magma. Mantle polymict breccias occurring as xenoliths in several kimberlites have commonly been linked to an early stage of kimberlite magmatism (Giuliani et al. 2014 and references therein). In a study of Bultfontein kimberlite, Giuliani et al. (2016) suggested high pressure crystallisation of phlogopite 'antecrysts' at various mantle depths by previous 'failed' kimberlite activity. These studies clearly suggest that multiple pulses of magma have contributed to the final mineral contents and compositions of kimberlites and ultramafic lamprophyres. The deformed olivine-IIIa phenocrysts from P4 are similarly interpreted to have crystallised from an earlier pulse of magma at mantle depth.

Olivine-IIIb overgrowth rims: low pressure crystallisation

The presence of inclusions of groundmass phases such as phlogopite, perovskite and spinel in the olivine-IIIb overgrowth rims from P4 indicate concurrent crystallisation of both olivine and the groundmass phases at a late stage in the eruption of magmas. The overgrowth rims from P3 show "decoupled behavior" of minor elements (decreasing Ni and fluctuating Ca, Cr and Mn) with respect to a near-constant Fo content which is similar to that reported from melt trend olivines (e.g. Kamenetsky et al. 2008; Arndt et al. 2010; Pilbeam et al. 2013; Bussweiler et al. 2015). Such uniform Fo composition of the rim implies buffering of the magma at a constant Fe^{2+}/Mg (Mitchell 1986), which is thought to be possible in the carbonate-rich P3 kimberlite if the Mg–Fe distribution coefficient between olivine and a carbonate–silicate melt is significantly higher than that for common basaltic systems (Kamenetsky et al. 2008). On the other hand, the Mg–Fe in the carbonate-poor P4 lamproite is only partially buffered which can be explained by fractional crystallization of olivine either coupled with assimilation of orthopyroxene (Pilbeam et al. 2013) or without such assimilation if a high olivine–melt partition coefficient ($D_{Ni} > 20$) is considered (Foley and Jenner 2004; Cordier et al. 2015). Fluctuations in Ca, Cr and Mn contents observed in the overgrowth rims can arise from several factors including changes

in environmental conditions such as magma composition or to differences in growth rate vs diffusion in the melt (Shore and Fowler 1996).

Olivine-IIIb overgrowth rims from P3 can generally be differentiated from those from P4 by their lower Ca, Al and Cr contents. However, an enigmatic aspect of P3 is the crystallisation of late-stage olivine with extraordinarily Mg-rich composition accompanied by very high Ca and Mn and low Ni contents as noted from the inclusion in monticellite. Similar olivine compositions have been described in previous studies on kimberlite where high-Mg rinds form the outermost part of olivine grains (Fedortchouk and Canil 2004; Kamenetsky et al. 2008; Arndt et al. 2010; Brett et al. 2009; Pilbeam et al. 2013; Bussweiler et al. 2015; Howarth and Taylor 2016). Such Mg-rich olivine compositions can result from equilibration with late-stage carbonatitic fluids (Pilbeam et al. 2013) or crystallisation from residual kimberlite melts at unusually high oxidation state (fO_2) because Fe in the ferric state is too large to be incorporated in olivine (Fedortchouk and Canil 2004; Bussweiler et al. 2015). The latter is a plausible scenario in P3 since the spinel evolution to magnesio-ulvöspinel-magnetite and then magnetite (Fig. 6a) indicates the prevalence of high fO_2 towards the late stage of magmatic evolution.

Olivine-IIIc alteration rims and zones

Olivine-IIIc alteration rims and zones (Fo 87–90) have developed by the interaction of Fe-rich melt with Mg-rich olivine-I (Fo 90–93). Howarth and Taylor (2016) reported the development of Fe-rich alteration zone surrounding a polycrystalline Mg-rich olivine and termed it as diffusive equilibration zone. However, the solid-melt system may not have achieved chemical equilibrium and hence it is more appropriate to call these zones as alteration rims and zones.

The presence of intragranular fractures cross-cutting the higher Fo cores, which have alteration zones with compositions similar to the overgrowth zones, suggest that the melt at this stage was able to intrude along these fractures. Similar fractures have been reported for olivines in kimberlites from Canada (Brett et al. 2015) and South Africa (Howarth and Taylor 2016) and interpreted to result from rapid decompression during ascent. Therefore, the alteration zones develop en route to the surface during transport by the ascending magma. Unusual enrichment of Ca and Mn in the olivine-IIIc M2 trend is possibly the result of interaction with a late-stage residual melt (e.g. Pilbeam et al. 2013).

Distinction between neoblasts and phenocrysts of olivine

Unaltered neoblasts developed from olivine-I macrocrysts in P4 have the same Mg-rich composition as the parent crystal. However, when altered to Fe-rich compositions by solid–melt interaction, the neoblasts may be confused with true phenocrysts of olivine-IIIa because of morphological similarity and one way to distinguish them is by using the Fe–Mg zoning pattern. Phenocrysts show increasing Mg from the core to the rim, while altered neoblasts exhibit the opposite because their Mg-rich core composition is inherited from the parent crystal and their rim is Fe-rich due to solid–melt interaction. Phenocrysts contain inclusions of magmatic spinel, albeit rarely, which will be absent in neoblasts. Another aspect of olivine-IIIa phenocrysts is their plastic deformation, though it is limited to a few grains. Olivine neoblasts (Brett et al. 2009) and tablets (Arndt et al. 2010) are essentially strain-free because they develop by the process of recovery (Passchier and Trouw 2005). However, there is no reason why the neoblasts cannot be deformed later during their transport by the host magma in the same way as the olivine-IIIa phenocrysts.

Evolution of kimberlite and lamproite magmas

The key observation in this study is the association of olivines of different paragenesis with other minerals such as mica and clinopyroxene (Table 2). We provide evidence that the relatively Fe-rich olivines formed from precursor melts of the intrusions along with phlogopite in kimberlite and clinopyroxene in lamproite in the respective mantle source regions. In P4, this was followed by crystallisation of olivine phenocrysts at mantle depths from an early pulse of magma, and an episode of solid-laden viscous magmatic flow during which some of the olivine phenocrysts underwent plastic deformation. Thereafter, the magma ascended rapidly. Crystallisation of groundmass occurred at crustal levels during which olivine grew on pre-existing olivine crystals as discrete overgrowth rims along with occasional inclusions of some of the groundmass minerals. Solid–melt interaction at various stages of magmatic evolution resulted in the alteration of pre-existing Mg-rich olivine crystals to Fe-rich compositions along the rims and intragranular fractures.

In P3, Fe-rich olivine macrocysts extend to much lower Fo composition compared to P4 which is possibly because they formed along with phlogopite. Crystallisation of olivine phenocrysts and development of alteration rims in P3 remain unconstrained because of extensive serpentinisation of olivine crystals. However, overgrowth rims of olivine record crystallisation from Fe^{2+}–Mg buffered magma which is attributed to the carbonate-rich nature of the magma.

Although P3 and P4 intrusions are located in close proximity and are temporally equivalent, one is a kimberlite and the other lamproite. The close spatial association of kimberlites, lamproites and ultramafic lamprophyres in the WKF

Table 2 Olivine, clinopyroxene and phlogopite types from intrusions P3 and P4

Type/subtype		P3 kimberlite	P4 lamproite
Type-III Magmatic crystals, rims and alteration zones	Type-IIIc: Alteration by solid–melt interaction		Olivine-IIIc (Fo 87–90; trend M1 with high Ni, Ca, Mn; trend M2 with low Ni, very high Ca, Mn): alteration rim on olivine-I macrocrysts; alteration zone adjacent to intragranular fractures and recrystallised parts of olivine-I macrocrysts; altered neoblasts
	Type-IIIb: Low pressure crystallisation	Olivine-IIIb (Fo 88–89; low Ni; low to high Ca; high Co, Mn): overgrowth rim on olivine-I core; unusual inclusion in monticellite (Fo 96; very low Ni; very high Ca, Mn) Clinopyroxene-IIIb[a] (low Al, Cr, Ti): fine-grained aggregates near crustal xenoliths, but absent from the groundmass Phlogopite-IIIb (low Cr–low Ti–high Ba): microphenocrysts with inclusions of other groundmass phases; tiny needles in groundmass	Olivine-IIIb (Fo 87–90; low to high Ni; high Ca, Co, Mn): overgrowth rim on olivine-I and olivine-II cores with occasional inclusions of groundmass spinel Clinopyroxene-IIIb (low Al, Cr; low to high Ti): microphenocrysts; groundmass crystals Phlogopite-IIIb (low Cr–moderate Ti–moderate Ba): poikilitic laths with inclusions of other groundmass phases
	Type-IIIa: High pressure crystallisation		Olivine-IIIa (Fo 85–90; high Ni, Ca, Co, Mn): phenocrysts and microphenocrysts, some of which are deformed; rarely contain spinel inclusions
Type-II crystals, nodules and rims Possibly cognate, genetically linked to a precursor melt in the mantle source region		Olivine-II (Fo 81–89; low Ni; low to high Ca; high Co, Mn): macrocrysts rarely containing inclusions of ilmenite Phlogopite-II (high Cr–high Ti–moderate Ba): overgrowth on phlogopite-I core of a deformed grain; lining of intergranular boundaries in glimmerite nodules of phlogopite-I	Olivine-II (Fo 85–87; low Ni; high Ca, Co, Mn): macrocrysts and megacrysts; olivine–clinopyroxene nodule Clinopyroxene-II (moderate Al, high Cr, low Ti): olivine–clinopyroxene nodule; inclusions in olivine-II megacrysts
Type-I crystals and nodules Xenocrysts and xenoliths inherited from the mantle		Olivine-I (Fo 90–93; high Ni; low Ca, Co, Mn): macrocrysts Clinopyroxene-I (moderate Al and Cr, low Ti): highly resorbed macrocrysts; relicts in altered phlogopite–clinopyroxene nodules Phlogopite-I (high Cr–low Ti–low Ba): deformed macrocrysts seldom intergrown with vermicular spinel; glimmerite and phlogopite–clinopyroxene nodules	Olivine-I (Fo 91–93; high Ni; low Ca, Co, Mn): macrocrysts with inclusions of orthopyroxene and aluminous magnesiochromite; development of mosaic texture and neoblasts in recrystallised parts of macrocrysts

[a]Formed from contaminated melt and not considered a primary phase

and their near contemporaneous emplacement at ~ 1100 Ma (Shaikh et al. 2017) call for a unifying model which can account for the genesis of diverse magmas from a variety of geochemical reservoirs. It has been proposed by several workers that silica-undersaturated carbonatite-like melts assimilate mantle minerals, especially orthopyroxene to produce kimberlitic melt and olivine saturation (Russell et al. 2012; Kamenetsky and Yaxley 2015 and references therein). In order to explain the development of different magma compositions in this process, Tappe et al. (2008, 2011) proposed that an asthenosphere-derived carbonatite-like melt interacts with variably metasomatised source regions in the sub-continental lithospheric mantle (SCLM). Pilbeam et al. (2013) suggested that variation in magma composition can further arise due to the digestion of different types of the xenolithic and xenocrystic load during ascent through the lithosphere. Soltys et al. (2016) documented assimilation of clinopyroxene and garnet by kimberlitic melts. For P3 kimberlite, which contains resorbed nodules of glimmerite and phlogopite–clinopyroxene, an assimilation reaction of the following type is suggested:

Silica-poor carbonatite melt + orthopyroxene
+ clinopyroxene + phlogopite
= olivine + carbonated silicate melt

One of the main differences in the groundmass mineralogy of P3 and P4 is the occurrence of monticellite in P3 and clinopyroxene in P4. This is clearly the result of higher silica activity in the P4 magma which can develop if the proportion of silica-rich phases such as phlogopite and clinopyroxene participating in the above assimilation reaction is high. Such an explanation is consistent with the findings of Giuliani et al. (2015) who invoked MARID-veined peridotites as the mantle source for orangeite magmas in southern Africa. Similarly, Ammannati et al. (2016) ascribed the origin of lamproites and leucitites in the Mediterranean alkaline field to differences in the SCLM lithology. This leads us to believe that the metasomatised wall rock for P4 lamproite was marked by a relative abundance of phlogopite-rich and MARID-type metasomatic veins (Tappe et al. 2008, 2011), while that for P3 kimberlite was refractory in nature.

Conclusions

Mineralogically, P3 rock is classified as phlogopite–monticellite kimberlite, while P4 is an olivine lamproite of unusual composition. Based on microtextures and compositions, three distinct populations of olivine, phlogopite and clinopyroxene are recognised. The first population includes glimmerite and phlogopite–clinopyroxene nodules from P3, and Mg-rich olivine macrocrysts (Fo 90–93) from both P3 and P4. This population is interpreted to be derived from disaggregated mantle rocks. The second population comprises macrocrysts of phlogopite and Fe-rich olivine (Fo81–89) from P3, megacrysts and macrocrysts of Fe-rich olivine (Fo85–87) from P4, and a rare olivine–clinopyroxene nodule from P4. Overlapping major and minor element compositions indicate that the megacrysts, macrocrysts and nodule of the second population have a common origin and a genetic link with a precursor melt of the respective intrusions. Minerals of the third population are clearly of magmatic origin and include Fe-rich euhedral phenocrysts of olivine crystallised at mantle depths, and olivine overgrowth rims formed contemporaneously with the groundmass at crustal levels. Among the three populations of phlogopite, the first is marked by high Cr–low Ti–low Ba compositions, while the second is of high Cr–high Ti–moderate Ba type. The third population exhibits low Cr–low Ti–high Ba composition in P3 and low Cr–moderate Ti–moderate Ba composition in P4. Multiple generations of olivine, phlogopite and clinopyroxene indicate a complex evolutionary history of the kimberlite and lamproite magmas. Close spatial association and contemporaneous emplacement of kimberlite and lamproite is explained by a unifying petrogenetic model which involves the interaction of a silica-poor carbonatite melt with differently metasomatised wall rocks in the lithospheric mantle. The metasomatised wall rock for P4 lamproite was characterised by abundant phlogopite-rich and MARID-type metasomatic veins, while that for P3 kimberlite was relatively refractory in nature.

Acknowledgements We are grateful to Geoffrey Howarth and Lynton Jaques for their detailed and valuable comments. Andrea Giuliani is thanked for editorial handling. The Department of Science and Technology, Government of India, provided the financial support (grant no. IR/S4/ESF-16/2009) for establishing the EPMA National Facility, Indian Institute of Technology Bombay, under the Intensification of Research in High Priority Areas (IRPHA) scheme.

References

Akella J, Rao PS, McCallister RH, Boyd FR, Meyer HOA (1979) Mineralogical studies on the diamondiferous kimberlites of Wajrakarur area, south India. In: Boyd FR, Meyer HOA (eds) Kimberlites, diatremes and diamonds: their geology, petrology and geochemistry. Am Geophys Union vol 1, Washington D.C., pp 172–177

Ammannati E, Jacob DE, Avanzinelli R, Foley SF, Conticelli S (2016) Low Ni olivine in silica-undersaturated ultrapotassic igneous rocks as evidence for carbonate metasomatism in the mantle. Earth Planet Sci Lett 444:64–74

Anil Kumar, Heaman LM, Manikyamba C (2007) Mesoproterozoic kimberlites in south India: a possible link to ~ 1.1 Ga global magmatism. Precambrian Res 154:192–204

Arndt NT, Guitreau M, Boullier AM, Le Roex A, Tommasi A, Cordier P, Sobolev A (2010) Olivine, and the origin of kimberlite. J Petrol 51:573–602

Brett RC, Russell JK, Moss S (2009) Origin of olivine in kimberlite: Phenocryst or impostor? Lithos 112:201–212

Brett RC, Russell JK, Andrews GDM, Jones TJ (2015) The ascent of kimberlite: insights from olivine. Earth Planet Sci Lett 424:119–131

Bussweiler Y, Foley SF, Prelevic D, Jacob DE (2015) The olivine macrocryst problem: new insights from minor and trace element compositions of olivine from Lac de Gras kimberlites. Canada Lithos 220:238–252

Carswell DA (1975) Primary and secondary phlogopites and clinopyroxenes in garnet lherzolite xenoliths. Phys Chem Earth 9:417–429

Chalapathi Rao NV, Gibson SA, Pyle DM, Dickin AP (2004) Petrogenesis of proterozoic lamproites and kimberlites from the cuddapah basin and Dharwar craton, southern India. J Petrol 45:907–948

Chalapathi Rao NV, Dongre A, Wu F-Y, Lehmann B (2016) A late cretaceous (ca. 90 Ma) kimberlite event in southern India: implication for sub-continental lithospheric mantle evolution and diamond exploration. Gondwana Res 35:378–389

Clement CR (1982) A comparative geologic study of some major kimberlite pipes in the Northern Cape and Orange Free State. Ph.D. Thesis. Department of Geology, University of Cape Town

Cordier C, Sauzeat L, Arndt NT, Boullier AM, Batanova V, Barou F (2015) Metasomatism of the lithospheric mantle immediately precedes kimberlite eruption: new evidence from olivine composition and microstructures. J Petrol 56:1775–1796

Dawson JB, Smith JV (1975) Chemistry and origin of phlogopite megacrysts in kimberlite. Nature 253:336–338

Erlank AJ, Waters FG, Hawkesworth CJ, Haggerty SE, Allsopp HL, Rickard RS, Menzies MA (1987) Evidence for mantle metasomatism in peridotite nodules from the kimberlite pipes, South Africa. In: Menzies MA, Hawkesworth CJ (eds) Mantle metasomatism. Academic Press, London, pp 221–311

Fedortchouk Y, Canil D (2004) Intensive variables in kimberlite magmas, Lac de Gras, Canada and implications for diamond survival. J Petrol 45:1725–1745

Foley SF, Jenner GA (2004) Trace element partitioning in lamproitic magmas — the Gaussberg olivine leucitite. Lithos 75:19–38

Foley SF, Prelevic D, Rehfeldt T, Jacob DE (2013) Minor and trace elements in olivines as probes into early igneous and mantle melting processes. Earth Planet Sci Lett 363:181–191

Ganguly J, Bhattacharya PK (1987) Xenoliths in Proterozoic kimberlites from southern India: petrology and geophysical implications. In: Nixon PH (ed) Mantle xenoliths. Wiley, p 249–265

Giuliani A, Kamenetsky VS, Kendrick MA, Phillips D, Wyatt BA, Maas R (2013) Oxide, sulphide and carbonate minerals in a mantle polymict breccia: Metasomatism by proto-kimberlite magmas, and relationship to the kimberlite megacrystic suite. Chem Geol 353:4–18

Giuliani A, Phillips D, Kamenetsky VS, Kendrick MA, Wyatt BA, Goemann K, Hutchinson G (2014) Petrogenesis of mantle polymict breccias: insights into mantle processes coeval with kimberlite magmatism. J Petrol 55:831–858

Giuliani A, Phillips D, Woodhead JD et al (2015) Did diamond-bearing orangeites originate from MARID-veined peridotites in the lithospheric mantle? Nat Commun 6:6837

Giuliani A, Phillips D, Kamenetsky VS, Goemann K (2016) Constraints on kimberlite ascent mechanisms revealed by phlogopite compositions in kimberlites and mantle xenoliths. Lithos 240–243:189–201

Giuliani A, Soltys A, Phillips D et al (2017) The final stages of kimberlite petrogenesis: petrography, mineral chemistry, melt inclusions and Sr-C-O isotope geochemistry of the Bultfontein kimberlite (Kimberley, South Africa). Chem Geol 455:342–356

Gurmeet Kaur, Mitchell RH (2013) Mineralogy of P2-West 'Kimberlite', Wajrakarur kimberlite field, Andhra Pradesh, India:kimberlite or lamproite? Mineral Mag 77:3175–3196

Gurmeet Kaur, Mitchell RH (2016) Mineralogy of the P-12 K-Ti-richterite diopside olivine lamproite from Wajrakarur,Andhra Pradesh, India: implications for subduction-related magmatism in eastern India. Miner Petrol 110:223–245

Gurmeet Kaur, Korakoppa M, Fareeduddin, Pruseth KL (2013) Petrology of P-5 and P-13 ''kimberlites'' from Lattavaram kimberlite cluster, Wajrakarur Kimberlite Field, Andhra Pradesh,India: reclassification as lamproites. In: Pearson DG, Grutter HS, Harris JW et al.(eds) Proceedings of the 10th IKC, Spl Issue J Geol Soc India vol 1, Bangalore, pp 183–194

Gurney JJ, Jakob WRO, Dawson JB (1979) Megacrysts from the Monastery kimberlite pipe, South Africa. 'The mantle sample: inclusion in kimberlites and other volcanics'. Am Geol Union Washington D.C., p 227–243

Hops JJ, Gurney JJ, Harte B (1992) The Jagersfontein Cr-Poor megacryst suite—towards a model for megacryst petrogenesis. J Volcanol Geotherm Res 50:143–160

Howarth GH, Taylor LA (2016) Multi-stage kimberlite evolution tracked in zoned olivine from the Benfontein sill, South Africa. Lithos 262:384–397

Kamenetsky VS, Yaxley GM (2015) Carbonate–silicate liquid immiscibility in the mantle propels kimberlite magma ascent. Geochim Cosmochim Acta 158:48–56

Kamenetsky VS, Kamenetsky MB, Sobolev AV, Golovin AV, Demouchy S, Faure K, Sharygin VV, Kuzmin DV (2008) Olivine in the Udachnaya-East kimberlite (Yakutia, Russia): types, compositions and origins. J Petrol 49:823–839

Kamenetsky VS, Golovin AV, Maas R, Giuliani A, Kamenetsky MB, Weiss Y (2014) Towards a new model for kimberlite petrogenesis: evidence from unaltered kimberlites and mantle minerals. Earth Sci Rev 139:145–167

Kargin AV, Sazonova LV, Nosova AA, Lebedeva NM, Tretyachenko VV, Abersteiner A (2017) Cr-rich clinopyroxene megacrysts from the Grib kimberlite, Arkhangelsk province, Russia: relation to clinopyroxene–phlogopite xenoliths and evidence for mantle metasomatism by kimberlite melts. Lithos 292–293:34–48

Kopylova MG, Nowell GM, Pearson DG, Markovic G (2009) Crystallization of megacrysts from protokimberlitic fluids: geochemical evidence from high-Cr megacrysts in the Jericho kimberlite. Proceedings of the 9th IKC, Lithos 112S:284–295

Kreston P (1973) The geology of Lemphane pipes and neighbouring intrusions. In: Nixon PH (ed) Lesotho kimberlites. Cape and Transvaal Printers, pp 159–167

Lim E, Giuliani A, Phillips D, Goemann K (2018) Origin of complex zoning in olivine from diverse, diamondiferous kimberlites and tectonic settings: Ekati (Canada), Alto Paranaiba (Brazil) and Kaalvallei (South Africa), Miner Petrol this volume

Lloyd FE, Woolley AR, Stoppa F, Eby GN (2002) Phlogopite–biotite parageneses from the K–mafic–carbonatite effusive magmatic association of Katwe–Kikorongo, SW Uganda. Miner Petrol 74:299–322

Mitchell RH (1986) Kimberlites: mineralogy, geochemistry and petrology. Springer Science & Business Media p 442

Mitchell RH (1995) Kimberlites, orangeites and related rocks. Plenum Press, New York, p 410

Mitchell RH, Bergman SC (1991) Petrology of lamproites. Plenum Press, New York, p 447

Moore A, Costin G (2016) Kimberlitic olivines derived from the Cr-poor and Cr-rich megacryst suites. Lithos 258–259:215–227

Nehru CE, Reddy AK (1989) Ultramafic xenoliths from Wajrakarur kimberlites, India. In: Ross J, Jaques AL, Ferguson J et al. (eds)

Kimberlites and Related Rocks, Proceedings of the 4th IKC, Geol Soc Australia Spl Pub vol 14, Sydney, pp 745–759
Passchier CW, Trouw RAJ (2005) Microtectonics. Springer, Berlin, p. 353
Pilbeam LH, Nielsen T, Waight TE (2013) Digestion fractional crystallization (DFC): an important process in the genesis of kimberlites. Evidence from olivine in the Majuagaa kimberlite, southern West Greenland. J Petrol 54:1399–1425
Ramakrishnan M, Vaidyanadhan R (2008) Geology of India. Geol Soc India 1, Bangalore, 556
Rao PS, Phadtre PN (1966) Kimberlite pipe-rocks of Wajrakarur area Anantapur district, Andhra Pradesh. J Geol Soc India 7:118–123
Ravi S, Sufija MV, Patel SC, Sheikh JM, Sridhar M, Kaminsky FV, Khachatryan GK, Nayak SS, Bhaskara Rao KS (2013) Diamond potential of the Eastern Dharwar Craton, southern India, and a reconnaissance study of physical and infrared characteristics of the diamonds. In: Pearson DG, Grutter HS, Harris JW et al. (eds) Proceedings of the 10th IKC, Spl Issue J Geol Soc India vol 1, Bangalore, p 335–348
Reddy TAK (1987) Kimberlite and lamproitic rocks of Wajrakarur area, Andhra Pradesh. J Geol Soc India 61:131–146
Russell JK, Porritt LA, Lavallée Y, Dingwell DB (2012) Kimberlite ascent by assimilation-fuelled buoyancy. Nature 481:352–356
Scott Smith BH (1989) Lamproites and kimberlites of India. Neues Jb Mineral Abh 161:193–225
Shaikh AM, Patel SC, Ravi S, Behera D, Pruseth KL (2017) Mineralogy of the TK1 and TK4 "kimberlites" in the Timmasamudram cluster, Wajrakarur Kimberlite Field, India: implications for lamproite magmatism in a field of kimberlites and ultramafic lamprophyres. Chem Geol 455:208–230
Shore M, Fowler AD (1996) Oscillatory zoning in minerals: a common phenomenon. Can Mineral 34:1111–1126
Skinner EMW (1989) Contrasting Group I and Group II kimberlite petrology: towards a genetic model for kimberlites. In: Ross J, Jaques AL, Ferguson J et al. (eds) Kimberlites and Related Rocks, Proceedings of the 4th IKC, Geol Soc Australia Spl Pub vol 14, Sydney, p 528–544
Soltys A, Giuliani A, Phillips D, Kamenetsky VS, Maas R, Woodhead J, Rodemann T (2016) In-situ assimilation of mantle minerals by kimberlitic magmas — direct evidence from a garnet wehrlite xenolith entrained in the Bultfontein kimberlite (Kimberley, South Africa). Lithos 256–257:182–196
Su BX, Zhang HF, Sakyi PA et al (2011) The origin of spongy texture in minerals of mantle xenoliths from the Western Qinling, central China. Contrib Mineral Petrol 161:465–482
Tappe S, Foley SF, Kjarsgaard BA, Romer RF, Heaman LM, Stracke A, Jenner GA (2008) Between carbonatite and lamproite—diamondiferous Torngat ultramafic lamprophyres formed by carbonate-fluxed melting of cratonic MARID-type metasomes. Geochim Cosmochim Acta 72:3258–3286
Tappe S, Pearson DG, Nowell G, Nielsen T, Milstead P, Muehlenbachs K (2011) A fresh isotopic look at Greenland kimberlites: cratonic mantle lithosphere imprint on deep source signal. Earth Planet Sci Lett 305:235–248
Veter M, Foley SF, Mertz-Kraus R, Groschopf N (2017) Trace elements in olivine of ultramafic lamprophyres controlled by phlogopite-rich mineral assemblages in the mantle source. Lithos 292–293:81–95